



GLOBAL JOURNAL OF SCIENCE FRONTIER RESEARCH
PHYSICS AND SPACE SCIENCE
Volume 13 Issue 4 Version 1.0 Year 2013
Type : Double Blind Peer Reviewed International Research Journal
Publisher: Global Journals Inc. (USA)
Online ISSN: 2249-4626 & Print ISSN: 0975-5896

Higher Order DNS on an Airfoil Fx77-W500 using Spectral/Hp Method

By M. M. Hossain, B. Stoevesandt & J. Peinke

Pabna University of Science & Technology, Bangladesh

Abstract - The prediction of aerodynamic properties of thick airfoils is a tricky business for the blade manufactures. Computational fluid dynamics (CFD) offers a number of significant advantages to investigate the flow properties around airfoils, however, most turbulence models are working properly except having some problems in case of turbulent separation. The spectral/hp elements method offers fast convergence due to the better resolution in a short time. Therefore, we perform direct numerical simulation (DNS) at the Reynolds number (Re) = 3900, polynomial orders (P)=9 and an angle of attack of $\alpha = 12^\circ$ round an airfoil (Fx77-W500) using spectral/hp elements method to solve the unsteady, viscous and two dimensional (2D) incompressible Navier- Stocks equations. A frequent fluctuation of the lift and drag forces has been found over the entire time. The contour plots of pressure and velocity magnitude around the airfoil are investigated for certain cases, which show more vortices at the upper portion of the airfoil and around the trailing edge. The presented results show that some interesting and peculiar behaviors due to unsymmetrical airfoil shape, which remind more of a bluff body, that the lift forces show negative value very frequently.

Index terms : reynolds number (RE), direct numerical simulation (DNS), spectral/hp elements method, polynomial orders (P), forces, contour plots.

GJSFR-A Classification : FOR Code: 090101



Strictly as per the compliance and regulations of :



Higher Order DNS on an Airfoil Fx77-W500 using Spectral/Hp Method

M. M. Hossain ^α, B. Stoevesandt ^σ, & J. Peinke ^ρ

Abstract - The prediction of aerodynamic properties of thick airfoils is a tricky business for the blade manufactures. Computational fluid dynamics (CFD) offers a number of significant advantages to investigate the flow properties around airfoils, however, most turbulence models are working properly except having some problems in case of turbulent separation. The spectral/hp elements method offers fast convergence due to the better resolution in a short time. Therefore, we perform direct numerical simulation (DNS) at the Reynolds number (Re) = 3900, polynomial orders (P)=9 and an angle of attack of $\alpha=12^\circ$ round an airfoil (Fx77-W500) using spectral/hp elements method to solve the unsteady, viscous and two dimensional (2D) incompressible Navier-Stocks equations. A frequent fluctuation of the lift and drag forces has been found over the entire time. The contour plots of pressure and velocity magnitude around the airfoil are investigated for certain cases, which show more vortices at the upper portion of the airfoil and around the trailing edge. The presented results show that some interesting and peculiar behaviors due to unsymmetrical airfoil shape, which remind more of a bluff body, that the lift forces show negative value very frequently.

Indexterms : reynolds number (RE), direct numerical simulation (DNS), spectral/hp elements method, polynomial orders (P), forces, contour plots.

I. INTRODUCTION

Wind turbines (WT) are used for extracting kinetic energy from wind and generate a significant growing factor of the world's energy demand, and offer a promise for inexpensive and clean energy. The foremost aims of the most wind turbines are to extract as much energy as possible from wind, and the each component of WT has to be optimized for that goal. Therefore, suitable blade geometry is needed to achieve maximum power coefficient. Due to the turbulent nature of wind, the prediction of aerodynamic and aero acoustic properties of WT is a major concerning threats for engineers (e.g. involving wind gusts, turbulence, icing), which affect turbine performance (energy output, noise emission etc), life expectancy and safety, see Tony et al. [1].

Author α : Department of Electrical and Electronic Engineering, Pabna University of Science & Technology, Pabna-6600, Bangladesh.
E-mail : motahertex@yahoo.com

Author σ ρ : Institute of Physics and ForWind, Carl von Ossietzky University Oldenburg, D-26111 Oldenburg, Germany.
E-mails : bernhard.stoevesandt@uni-oldenburg.de, peinke@uni-oldenburg.de

Considering the factors, conducting experiment on such type problem is much more expensive, computational fluid dynamics (CFD) modeling and experiments are interesting alternative. This method has both advantages and disadvantages. Nevertheless, CFD provide more detailed and comprehensive information and is increasingly cost effective than wind tunnel test. On the other hand, CFD consume less energy, by Fletcher [2]. There are several methods to simulate turbulence flow such as: direct numerical simulation(DNS), large eddy simulation(LES), Reynolds averaged Navier-Stocks model (RANS model), Reynolds stress models, very large eddy simulation, detach eddy simulation, vortex method, Vorticity conformed method, two phase method, see Ferziger and Peric [3]. Bernhard St. et al. [4], performed two dimensional simulation using the spectral element code on fx79-w151a airfoil at moderate Reynolds number $Re=33000$ and at angle of attack 120° . Their result suggested that vortex shedding appear in front of the airfoil and was confirmed by HPIV measurement. In another work, Bernhard St. et al. [5] investigated that the effects of dynamic stall using spectral/hp code on the same airfoil [4] at $Re=11111$ and initial angle of attack of 120° . They found that the spectral element code is promising in simulating turbulent flows using DNS and LES. Dong et al. [6] inspected the effects of the Reynolds number on the statistical characteristics of the cylinder wake and on the share-layer instability in the transition range. Both PIV measurements and DNS were performed at Reynolds number $Re=3900/4000$ and 10000 and found all the quantitative patterns move upstream with increasing Reynolds number, and high frequency fluctuation caused by share layer vortices for both cases. Another study made by Monty and Chong in [7] on a comparison between stream wise velocity data from experiment and DNS. The results showed that there were excellent agreements between the stream wise velocity statistics of the two data sets. The spectra are also very similar, however, throughout the logarithmic region the secondary peak in energy is clearly reduced in the DNS results. Therefore, we perform DNS on the airfoil (FX77-W500) using spectral/hp method to provide a prospect for aerodynamic control of modern wind turbine.

In section II, the analytical descriptions of the numerical methods are introduced including the spectral/hp element approach. The numerical setup is

discussed in section III. Simulating results are presented in section IV. Discussion and conclusions are given in section V.

II. THE NUMERICAL METHOD

The solver which is used for the numerical simulation is spectral element based solver called *Nektar*. It is a DNS solver. It provides fast convergence, small diffusion and dispersion errors, easier implementation of the in-sup condition for incompressible Navier-Stokes, and better data volume over-surface-ratio for efficient parallel processing and also better input/output handing due to the smaller volume of data. Since wind turbines are operating for low wind speed, it is enough to consider incompressible flows for DNS. The governing equations are the Navier-Stokes equations for incompressible, transient (or unsteady) and viscous flow can be written in dimensional form as:

$$\nabla \cdot \mathbf{u} = 0 \tag{1}$$

$$\frac{\partial \mathbf{u}}{\partial t} + (\mathbf{u} \cdot \nabla) \mathbf{u} = -\nabla p + \nu \nabla^2 \mathbf{u} + \mathbf{F} \tag{2}$$

where \mathbf{u} is stand for the velocity vector, P is the pressure, \mathbf{F} is the external forces and ν is the kinematics viscosity. The procedures used in *Nektar* consider a solution domain Ω (where Ω is a domain of \mathbb{R}^2) and which is decomposed into N_{el} elemental domains Ω^e such that

$$\Omega = \bigcup_{e=1}^{N_{el}} \Omega^e, \quad \text{Where} \quad \bigcap_{e=1}^{N_{el}} = \emptyset, \tag{3}$$

For the solution domain $\Omega = \{x \mid 0 < x < l\}$ a specific mesh can be denoted by points

$$0 = x_0 < x_1 < \dots < x_{N_{el}-1} < x_{N_{el}} = l \tag{4}$$

Therefore, the domain is defined as:

$$\Omega^e = \{x \mid x_{e-1} < x < x_e\} \tag{5}$$

and grid is obtained by partitioning the physical domain. One of the main reasons of using unstructured expansion for time dependent computations is rotationally symmetric considerations which increase the numerical efficiency, which was described by Sherwin et al [8]. More efficient numerical operation can be achieved by using expansions. The spectral expansion is being employed into each sub domains. A function $\Phi(x, y)$ over the e^{th} sub-domains can be represented a polynomial basis, $\psi_{i,j}(r, s)$ where $\Phi(x, y)$ can be written as:

$$\Phi(x, y) = \sum_e \sum_i \sum_j \Phi_{i,j}^e \psi_{i,j}(r, s). \tag{6}$$

Where the expansion coefficients for the polynomial are defined by $\Phi_{i,j}^e$ and (r, s) are the local

coordinate within the sub-domains. e^{th} The spatial/global coordinates can be defined as. (x, y) This extends the expansion bases within a standard region into multi domain expansion. Sherwin et al. [8] showed that to develop a suitable tensorial type basis within unstructured regions, such as the triangle, it is needed to develop a new coordinate system where the local coordinates have independent bounds. The advantage of such a system is that it can then define one-dimensional functions upon which we can construct our multi-domain tensorial basis. It also defines an appropriate system upon which we can perform important numerical operations such as integration and differentiation. Richard et al. [9] reported that the main drawback of spectral method is their inability to handle complex geometries and these complex geometries can easily be handled in triangular based spectral method.

A good assumption is standard triangular domain (Tri_{st}) system which is described by Sherwin [8, 10] such that,

$$Tri_{st} = \{ (r, s) \mid -1 \leq r, s; r + s \leq 0 \} \tag{7}$$

Now the local coordinate system (r, s) can be mapped for defining the global coordinate system (x, y) as

$$x = -\frac{(r+s)}{2}V_1 + \frac{(1+r)}{2}V_2 + \frac{(1+s)}{2}V_3 \tag{8}$$

Where the $V_1(-1,-1), V_2(1,-1)$, and $V_3(-1,1)$ are the physical coordinates of the vertices of the elementary (standard) triangle.

As the standard triangular domain is not independently bounded by the coordinates (r, s) , Sherwin et al. [8] introduced the so-called collapsed coordinate system (x, y) .

The collapsed Cartesian system is suitable for Gauss integration in the unstructured regions. The transformation to collapsed coordinate system can be interpreted as a mapping to a standard quadrilateral region (see Fig.1).

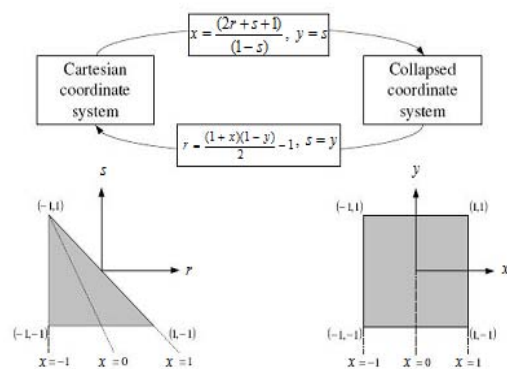


Figure1 : The standard triangular and collapsed coordinates

The transformation from $(r, s) \rightarrow (x, y)$ is given by:

$$x = \frac{(2r + s + 1)}{(1 - s)} \text{ and } y = s \quad (9)$$

The reverse transformation can be written as:

$$r = \frac{(1 + x)(1 - y)}{2} - 1 \text{ and } s = y \quad (10)$$

The standard triangle can now be defined in terms of collapsed coordinates as:

$$Tri_{st}^2 = \{ (x, y) \mid -1 \leq x, y \leq 1 \}, \quad (11)$$

The Spectral/hp method allows both h-type and p-type extensions. So, to construct p-type expansions, orthogonal polynomials have been considered. The Jacobi polynomials $P_n^{\alpha, \beta}(x)$ are an orthogonal set of polynomials in the interval $[-1, 1]$ with respect to the function $(1 - x)^\alpha (1 + x)^\beta$ where, $(\alpha, \beta > -1)$ can be defined as

$$P_n^{\alpha, \beta}(x) = \frac{(-1)^n}{2^n n!} (1 - x)^{-\alpha} (1 + x)^{-\beta} \frac{d^n}{dx^n} [(1 - x)^{\alpha+n} (1 + x)^{\beta+n}] \quad (12)$$

n stands for the polynomial order, and the coefficients α and β define the characterizing coefficient of the polynomial.

$P_n^{\alpha, \beta}(x)$ is Legendre polynomial $P_n^{0,0}(x)$ when $\alpha = \beta = 0$ and Chebychev polynomial can be obtained by imposing $\alpha = \beta = -\frac{1}{2}$. The orthogonal affiliation is important for the Jacobi polynomials and this can be written as

$$\int_{-1}^1 (1 - x)^\alpha (1 + x)^\beta P_i^{\alpha, \beta}(x) P_j^{\alpha, \beta}(x) dx = C \delta_{ij} \quad (13)$$

Where C depends on α, β , and i , and δ_{ij} is the Kronecker-Delta in which triangular sub-domains are mapped into a rectangular domain using mapping functions.

Finally full expansion basis which were already described by Dubiner [11], who considered a triangular basis as below:

$$\psi_{i,j}(r, s) = P_i^{0,0} \frac{(2r + s + 1)}{(1 - s)} (1 - s)^i P_j^{2i+1,0}(s) \quad (14)$$

Where i and j are the expansion orders which could be differing for different directions, and $P_i^{\alpha, \beta}$ denotes Jacobi Polynomials.

It is well known that the splitting method is a very popular approach to constructing efficient numerical methods for unsteady problems because it permits high-order time accuracy, Karniadakis et al. [12]. This approach is in common use in CFD as well. The splitting scheme used in the *Nektar* solver is a higher order time accurate scheme for the solution of

the incompressible Navier Stokes equations which was developed by Karniadakis et al. [12]. In their studies, incompressible flows with constant properties were considered, which are governed by the Navier-Stokes equations (1) and (2) written in the form,

$$\frac{\partial u}{\partial t} = -\nabla p + \nu L(u) + N(u) \quad \text{in } \Omega \quad (15)$$

subject to incompressible constraint

$$\Omega \equiv \nabla \cdot u = 0 \quad \text{in } \Omega \quad (16)$$

Where u is the velocity vector P , p is the pressure ν , is the kinematics viscosity. The linear and nonlinear operators are $N(u)$ and $L(u)$, respectively and can be defined as follows:

$$L(u) \equiv \nabla^2 \cdot u \quad (17)$$

$$N(u) \equiv -\frac{1}{2} [u \nabla \cdot u + \nabla(u \cdot u)] \quad (18)$$

The nonlinear terms are written here in a skew symmetry form in order to minimize aliasing effects. Finally, equation (17) is integrated, using high-order time-stepping schemes; such schemes are routinely used for the numerical solution of ordinary differential equations. The linear and nonlinear terms are approximated via implicit schemes for stability regions and explicit schemes for efficiency reasons, respectively and can be written in the integration form as:

$$\int_{t_i}^{t_{i+1}} L(u) dt = \Delta t \sum_{q=0}^{J_i-1} \gamma_q L(u^{l+1-q}), \quad (19)$$

$$\int_{t_i}^{t_{i+1}} N(u) dt \equiv \Delta t \sum_{q=0}^{J_e-1} \beta_q N(u^{l-q}) \quad (20)$$

Where γ_q and β_q are appropriately chosen weights for implicit and explicit schemes, respectively J_e and J_i are denote the explicit and implicit order of the scheme respectively. Karniadakis et al. [12] reported that the splitting scheme involves these steps as:

$$\frac{\hat{u} - u^l}{\Delta t} = \sum_{q=0}^{J_e-1} \beta_q N(u^{l-q}) \quad \text{in } \Omega \quad (21)$$

$$\frac{\hat{u} - \hat{u}}{\Delta t} = -\nabla p^{-l+1} \quad \text{in } \Omega \quad (22)$$

$$\frac{u^{l+1} - \hat{u}}{\Delta t} = \nu \sum_{q=0}^{J_i-1} \gamma_q L(u^{l+1-q}) \quad \text{in } \Omega, \quad (23)$$

Where,

$$\Delta t \nabla p^{-l+1} = \int_{t_i}^{t_{i+1}} \nabla p dt \quad (24)$$

III. NUMERICAL SETUP

The simulation of a flow over the profile (FX77-W-500) was undertaken and evaluated for several aspects such as force coefficients, the flow dynamics, vortices contours, and pressure contours. During the 2D simulation, the Reynolds number of 3900 and an angle of attack of $\alpha=120$, with polynomial orders $P = 9$ were chosen.

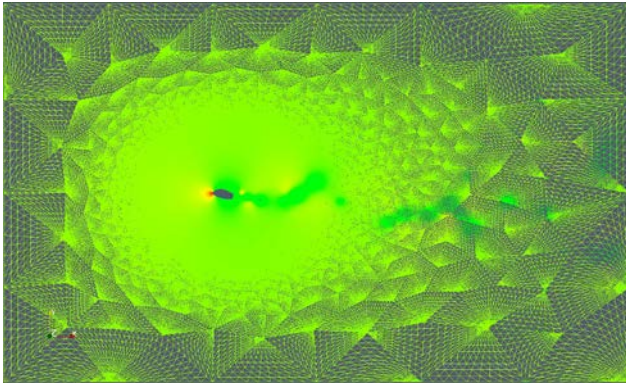


Figure 2 : Full mesh view with the polynomial nodes around the airfoil (FX77-W500)

Fig. 2 illustrates the used mesh with the polynomial nodes around an airfoil (FX77-W500). The unstructured grid was used throughout this work, the spectral/hp method employ permits the use of both structured and unstructured meshes, based on triangular and/or quadrilateral elements. The unstructured grid used was composed of 3814 triangular elements and 200 quadrilateral elements. The resolution of the grid was refined around the airfoil as well as in the wake region (Fig. 3 - 4) since the most interesting phenomenon was expected there; it already studied by Folkerts L. et al. [13] and Bernhard St. et al. [14].

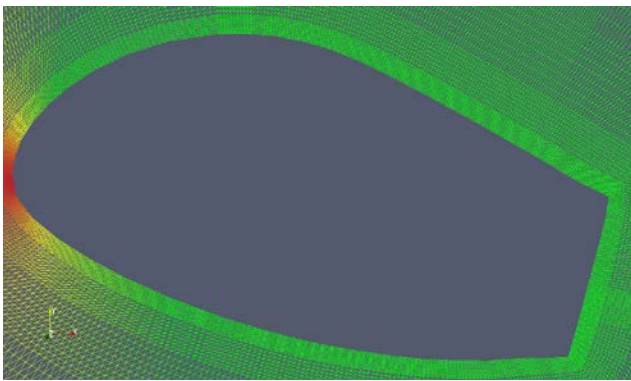


Figure 3 : Close-up view of the selected airfoil (FX77-W500)

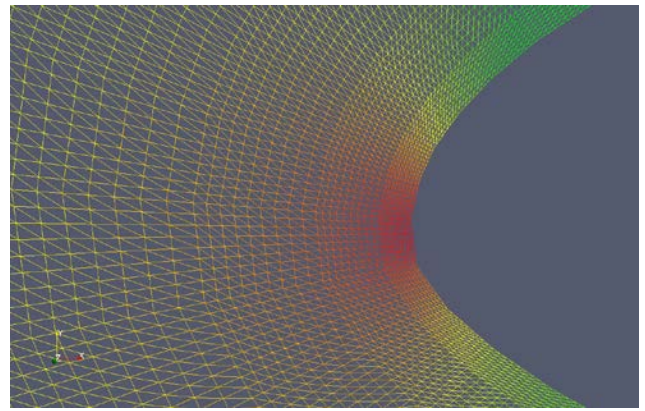


Figure 4 : Close-up view of the mesh around the leading edge of the airfoil with the polynomial nodes

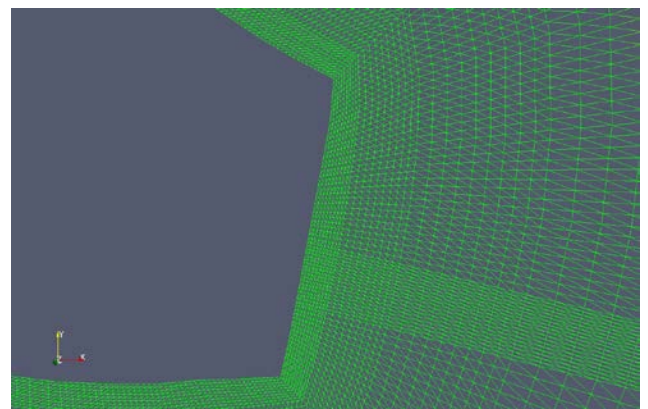


Figure 5 : Close-up view of the mesh around the tailing edge of the airfoil with the polynomial nodes

The computational domain extended from $-10C$ (C is the cord length of the profile) in the inflow direction to $20C$ in the out flow direction, and from $-10C$ to $10C$ in the cross flow direction. Hubscher [15] reported that specification of the time step is an essential parameter for the simulation because a too short time step can increase the computational cost. On the other hand, simulation could be crashed due to high velocity which is created around the leading edge of the airfoil for a too high time step. To achieve higher resolution, lower time step ($DT = 4 \cdot 10^{-5}$) considered during this work. The product of the time step and the number of time steps gives the required time units.

$$\text{Time units} = \text{time step} \times \text{number of steps} \quad (25)$$

This time units denotes that one time unit is needed for the flow to cover the distance of the chord length of the airfoil. The dimensionless time unit forms as:

$$t \rightarrow \frac{tU_0}{c} \quad (26)$$

Where U_0 is the free stream velocity and c is stand for chord length of the airfoil.

IV. SIMULATION AND RESULTS

The simulations were performed with an open source solver *Nektar* [16] which is developed by Sherwin et al. [8]. Paraview for visualization technique [17] was used to analyze the data. The force in the code is derived from equation (2) in section II as:

$$F = -\int_s Pnds + \int_s \tau.nds \tag{27}$$

The lift and drag forces and the flow dynamics, which are one of the most significant matters for the wind turbine blade designers. In Fig. 6 illustrates, the lift force (left side) and drag force (right side) over 80 dimensionless time units at $Re = 3900$, $\alpha = 12^\circ$ and $P=9$ which confirm the response of the lift and drag force to the turbulent separation at the blade surface. It has been seen that the lift forces (F_l) are not constant but highly unsteady. The average lift and drag forces coefficient are $F_{lmean} = 0.08528$ and $F_{dmean} = 0.2446$ respectively. The maximum drag $F_{dmax} = 0.6568$ is observed due to the high inertia at the time ($t = 0$) of simulation started and decreases to $F_{lmin} = 0.1124$ over the whole simulation period. The fluctuation of the lift is $F_{lmax} = 0.88610$ to $F_{lmin} = -0.76800$. At the time unit of $t = 2.156$, the lift forces has reached the maximum value $F_{lmax} = 0.88610$ due to the fact of a strong fast separation of vortices which occurs at the time unit of $t = 1.04$.

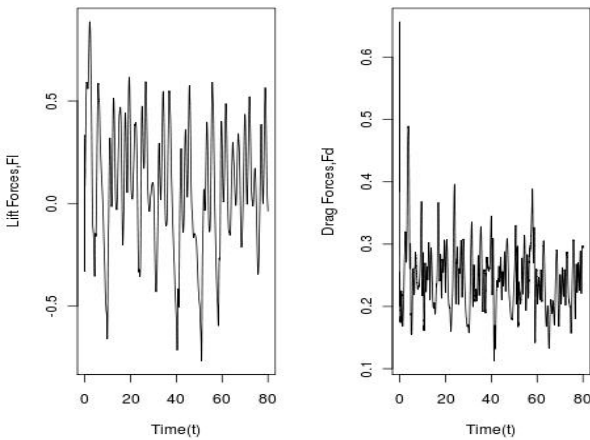


Figure 6 : Lift (left) and Drag (right) forces showing fluctuation over dimensionless time unit at $Re=3900$, $\alpha = 12^\circ$ and $P=9$ obtained using 2D *Nektar* solver

The standard deviation for the lift and drag forces are $F_{lstd} = 0.3052$ and $F_{dsts} = 0.0519$. The frequency of the vortex shedding could be described by the Strouhal Number (St), which is 0.15.

A screen shot of velocity magnitude contours is depicted in Fig. 7 that is modeled for the stationary airfoil (FX77-W500) when lift forces $F_l = 0$ at different time units $t = 32.00$ (in Fig. 7a) and $t = 46.00$ (in Fig.7b). It can be observed that the vortices are developed just

behind the upper portion of the trailing edge of the airfoil for both cases due to the fact of lift forces.

The leading edge structure is shown in light color and is a less effective area on the airfoil. The pressure contour plots in Fig. 8 explain the distribution of lift forces, when $F_l = 0$ as well. There is a low pressure contours just behind the trailing edge of airfoil that is shown in Fig. 8(b). A large area of low pressure contours is revealed in Fig. 8(a). These regions of low pressure are vortices that form, and detach from the airfoil. The leading edge structures are shown in lighter red colour with same graphical view for both cases.

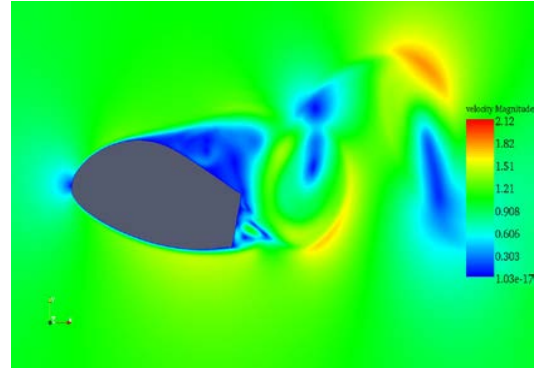


Figure 7(a) : Velocity magnitude contours and flow structure when the lift forces $F_l = 0$ and $t = 32.00$

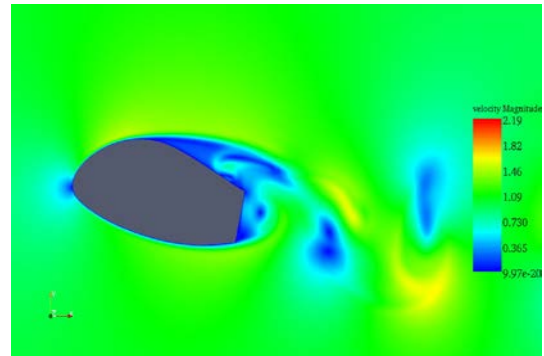


Figure 7(b) : Velocity magnitude contours and flow structure when the lift forces $F_l = 0$ and $t = 46.00$

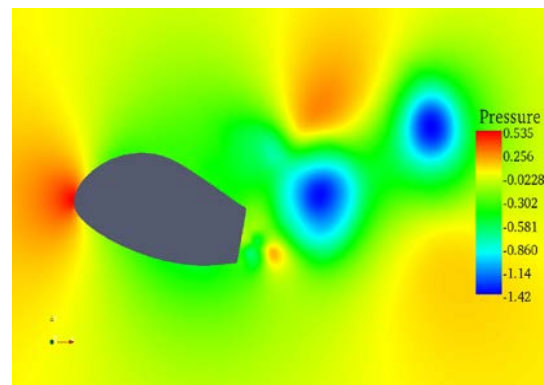


Figure 8(a) : Pressure contours and flow structure when the lift forces $F_l = 0$ and $t = 32.00$

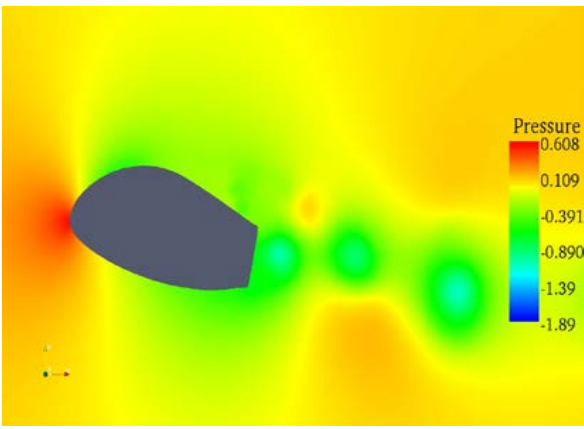


Figure 8 (b) : Pressure contours and flow structure when the lift forces $F_l = 0$ and $t = 46.00$

In the flowing Fig. 9 depict the velocity magnitude contour of the flow over the airfoil for $Re = 3900$ and $P = 9$ at $F_l = +0.54$ and $+0.57$ when time unit $t = 39.90$ (in Fig. 9a) and $t = 45.70$ (in Fig. 9b), respectively. While the leading edge flow structure shows the same structure compared to the $F_l = 0$ case, parabolic shaped vortices have been developed just behind the trailing edge, and are responsible for the maximum positive lift forces. In Fig. 10(a) and 10(b), the pressure distributions are shown. Two circles, one small and another one big size, develop just above the trailing edge. These two circles of low pressure are also responsible for the positive lift forces. The pressure at the leading edge of the airfoil show maximum values for both cases.

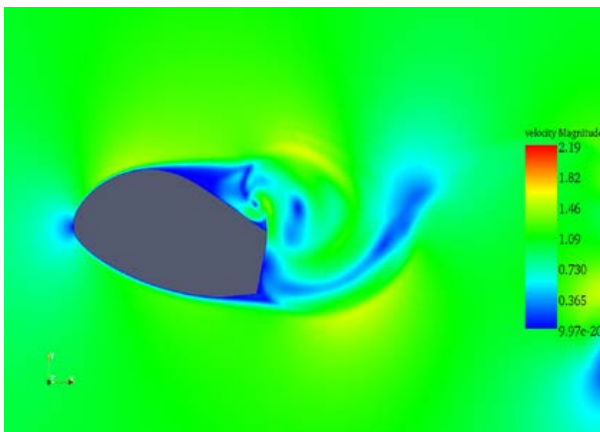


Figure 9 (a) : Velocity magnitude contours and flow structure when the lift forces $F_l = +0.54$ and $t = 39.90$

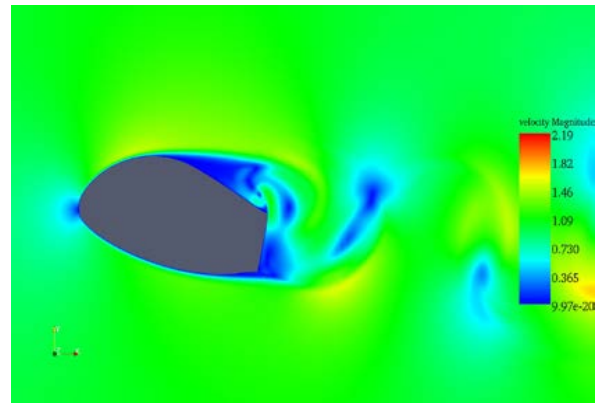


Figure 9 (b) : Velocity magnitude contours and flow structure when the lift forces $F_l = +0.57$ and $t = 45.70$

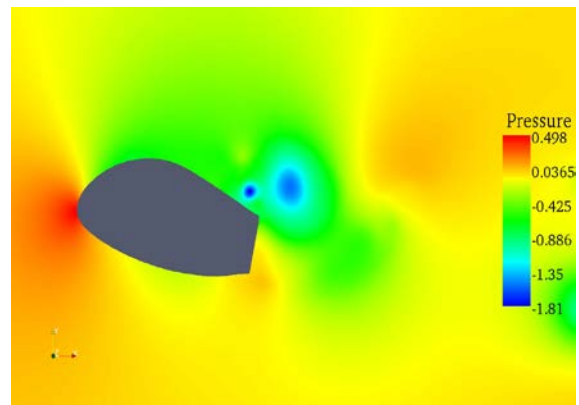


Figure 10 (a) : Pressure contours and flow structure when the lift forces $F_l = +0.54$ and $t = 39.90$

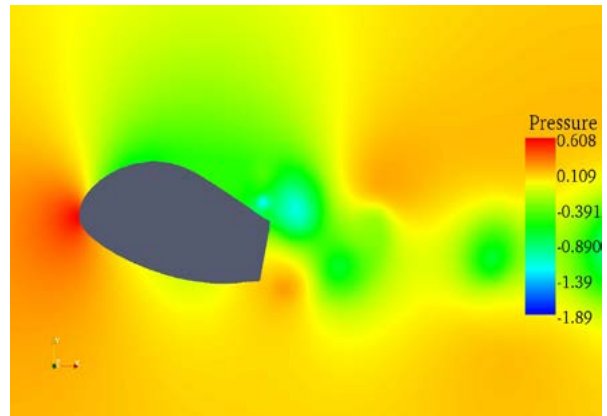


Figure 10 (b) : Pressure contours and flow structure when the lift forces $F_l = +0.57$ and $t = 45.70$

At the maximum negative lift forces $F_l = -0.71$ (in Fig. 11a) and -0.74 (in Fig. 11b), and the contours of velocity magnitude indicate at the time unit $t = 40.40$ and $t = 50.90$, respectively. The vortices just behind the trailing are completely opposite in structure when compared to the cases for positive lift forces. The separation has started at half chord length of the airfoil. Parabolic shaped vortices only at the upper part of the airfoil are responsible for the negative forces. One small

region of lower pressure is shown at the lower part of the trailing edge in Fig. 12(a). Another bigger region of the lower pressure is shown at the upper part of the trailing edge in Fig. 12(b). Combinations of both create vortices at the upper surface of the trailing edge and are responsible for lift forces.

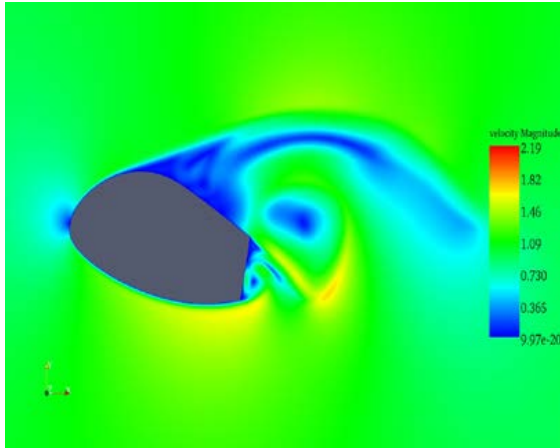


Figure 11(a) : Velocity Magnitude and flow structure when the lift forces $F_l = -0.71$ and $t = 40.40$

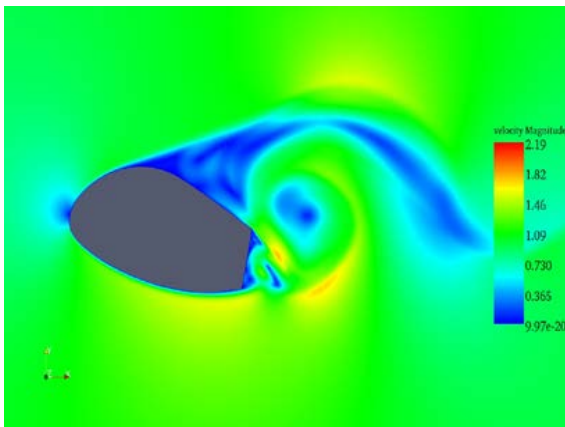


Figure 11 (b) : Velocity Magnitude and flow structure when the lift forces $F_l = -0.74$ and $t = 50.90$

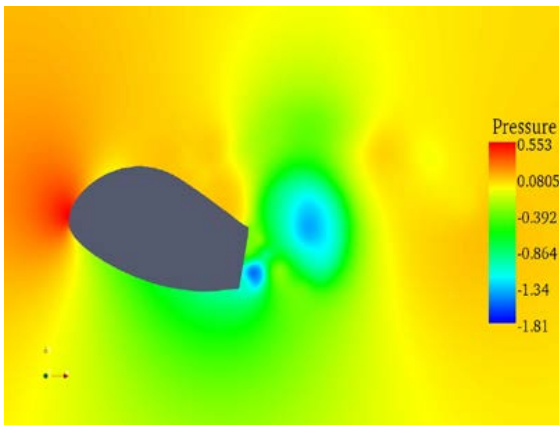


Figure 12 (a) : Pressure contours and flow structure when the lift forces $F_l = -0.71$ and $t = 40.40$

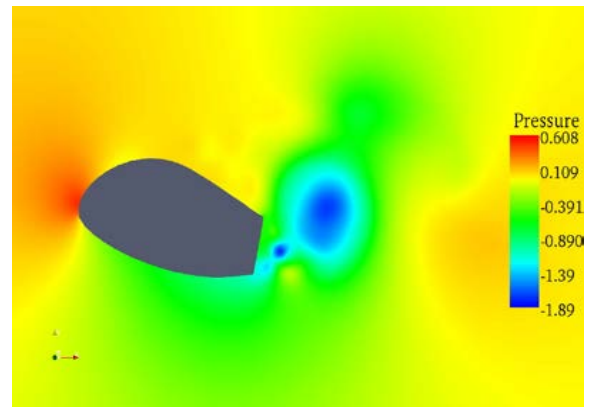


Figure 12 (b) : Pressure contours and flow structure when the lift forces $F_l = -0.74$ and $t = 50.90$

V. SUMMERY AND DISCUSSIONS

The direct numerical simulations(DNS) were used on a stationary airfoil (fx77-w500) using an open source CFD solver, Nektar, based on spectral/hp method. The simulations were done at Reynolds number $Re = 3900$ and polynomial order $P = 9$. The contour plots of velocity magnitude and pressure were analyzed and the flow structure investigated around the airfoil and the wake. More vortices in the wake region were identified. Further studies should be simulated for longer time units (at least up to 100 time units) for 2D simulations with the objective to maximize realistic results. A comparison between *Nektar* and with any other CFD solver should be included. In this paper, 3D simulations were not carried out, so the 3D could be done for further analysis. Finally, it is also suggested that since in this work stationary airfoil (fx77-w500) was used for angle of an attack of 120° . So, therefore it could be another option to do simulation for a different angle of attacks and for a moving airfoil.

ACKNOWLEDGEMENT

The authors like to take this opportunity to thank all of the colleagues in the Turbulence, Wind Energy and Stochastic (TWIST) group well known as ForWind research group at the Carl von Ossietzky University Oldenburg, D-26111 Oldenburg, Germany.

REFERENCES RÉFÉRENCES REFERENCIAS

1. Tony B., David S., Nick J., and Ervin B., "Handbook of Wind Energy", British Library Cataloguing in Publication Data, 2001.
2. Fletcher C A.J., "Computational Techniques for Fluid Dynamics" 1st and 2nd edition, 2006.
3. Ferziger J.H. and Peric M., "Computational Methods for Fluid Dynamics", 3rd edition, Springer, 2002.
4. Bernhard St., Christian St., Andrei Sh., Claus W. and Joachim P. , "Analysing Flow Structures around a Blade Using Spectral/hp Method and HPIV", Journal of Physics: Conference Series 75(2007) 012025.

5. Bernhard St., Andrei S., Joachim P. and Claus W., "Simulation Dynamic Stall Using a Spectral/hp CFD-Code", ECCOMAS CFD, 2004.
6. Dong S., Karniadakis G.E., Ekmekci A., and Rockwell D., "A Combined Direct Numerical Simulation–Particle Image Velocimetry Study of the Turbulent Near Wake", *J. Fluid Mech.*, 569:185–207, 2006.
7. Monty, J P. and Chong, M.S., "Turbulent Channel flow: Comparison of Streamwise Velocity Data from Experiments and Direct Numerical Simulation", *Journal of Fluid Mechanics*, 633:461-474, 2009.
8. Karniadakis G.E. and Sherwin S.J. "Spectral/hp Element Methods for CFD", 2nd edition, Oxford: Oxford University Press, 1999.
9. Richard P., Francesca R., "Spectral Element Methods on Triangles and Quadrilaterals: Comparisons and Applications", *Journal of Computational Physics*, 198:349–362, 2004.
10. Sherwin S.J. and Karniadakis G.E., "A Triangular Spectral Element method; Application to the incompressible Navier-Stokes Equation", *Computer methods in applied mechanics and engineering* 123 (1), 189-229, 1995.
11. Dubiner M., "Spectral Methods on Triangles and Other Domains", *Journal of Scientific Computing*, 6(4): 345-390, 1991.
12. Karniadakis G.E., Israeli M. and Orszag S.A., "High-order splitting methods for the incompressible Navier-Stokes equations", *Journal of Computational Physics*. 97:414–443, 1991.
13. Folkerts L. Barthelmie R. and et al. "Solar wind velocity measurement of offshore turbine wakes", *Wind Eng*; 25(5):301–306, 2010.
14. Bernhard St., Andrei S., Joachim P. and W. Claus, "Direct Numerical Simulation of the Turbulent Flow around an Airfoil Using Spectral/Hp Method", ECCOMAS CFD, 2006.
15. Hubscher N., "A user's guide to the felsia Nektar System" 1997.
16. <http://www.nektar.info/>
17. <http://www.paraview.org/>